THE ASTRONOMICAL JOURNAL VOLUME 111, NUMBER 2 FEBRUARY 1996

# DETECTION OF NEAR EARTH ASTEROIDS BASED UPON THEIR RATES OF MOTION

R. JEDICKE

Lunar & Planetary Laboratory, University of Arizona, Tucson, Arizona 85721
Electronic mail: jedicke@pirl.lpl.arizona.edu

*Received 1995 June 9; revised 1995 October 13*

## ABSTRACT

Spacewatch has been successfully discovering Near Earth asteroids (NEAs) for five years based upon the difference in the ecliptic rates of motion of these asteroids compared to their distant Main Belt, Trojan and Centaur cousins. The search for NEAs is usually restricted to regions on the sky near the ecliptic and opposition in order to take advantage of their increased brightness, the good correlation between the rates of motion and orbital elements, and their increased numbers in this direction. The present study introduces an analytic determination of the best location on the sky to search for NEAs based on their rate of motion. Assuming a reasonable orbit and magnitude-frequency distribution for NEAs, Main Belt, Mars crossing, Hungaria and Trojan asteroids, it is possible to derive the probability that an object moving with a specified rate in each direction at a given ecliptic latitude and longitude with respect to opposition is a NEA. The discovery probabilities are studied as a function of ecliptic latitude and longitude with respect to opposition, absolute magnitude of the discoverable NEAs, confidence level on the NEA detection, and limiting magnitude of the detection system. The discovery probabilities are examined for each of the NEAs discovered by Spacewatch. Imposing a 90% confidence level on the requirement that a candidate is a large NEA for a detection system with a limiting magnitude of $V=21$, it was found that scanning at opposition offers the best opportunity for NEA discovery. Discoveries are symmetric in the east-west direction about opposition due to an interesting inter-relation in the solutions for orbital elements of objects which may appear at the specified location. Detection systems with a fainter magnitude limit may find it better to scan about 45° from opposition in order to find the larger NEAs. 

## 1. INTRODUCTION

Spacewatch has enjoyed considerable success in the detection of NEAs based upon their rates of ecliptic motion relative to other asteroids (Gehrels & Jedicke 1995). The Steward Observatory's 0.9 m Spacewatch telescope on Kitt Peak and 2048×2048 Tektronix CCD provide a limiting magnitude of about 21. The system is utilized on every clear night during the dark time of each lunation.

Figure 1 shows the ecliptic latitude rate versus ecliptic longitude rate in degrees/day for asteroids from a simulated scan near opposition. Superposed on the plot is a rough outline of the identification of asteroids based upon their rates. Main Belt (MB) asteroids move at roughly one-quarter degree/day in longitude while more distant objects (Hilda, Trojan, Centaurs, etc.) move slower. The Hungarias are characterized by high inclination and are located inside the inner edge of the main belt; they often appear with high rates of motion in latitude and overall rates which might otherwise characterize them as NEAs. Mars-crossing asteroids often display longitudinal rates similar to the MB but with high latitude rates. The NEAs may appear anywhere on the plot and often mimic the rates of other asteroids. The key to their discovery is that they may also appear with distinctive rates identifying them as interesting objects.

Spacewatch observers currently use the solid boundary line in Fig. 1 to distinguish NEAs from other less interesting objects (Rabinowitz 1991). The curve was determined empirically from a simulation of asteroid-like orbits. They are asteroid-like in the sense that no single orbit used in the simulation was identical to the known orbit of any asteroid, but the ensemble of orbits was statistically similar to the known distribution. The figure has proven its merit for scans near opposition and even extending ±30° in longitude away from the antisolar point. As the scan region moves away from opposition the objects move more slowly. This causes a shift and compression of Fig. 1 which decreases its efficacy as the scan region approaches the stationary point. Under these circumstances the choice of objects to follow up falls more often upon the observer's experience rather than a quantitative measure of the likelihood that an object is a NEA. The rate of mistaken identifications increases correspondingly. Scanning is often forced into these undesirable locations when opposition is located in the Milky Way, where the automated software (Rabinowitz 1991) has difficulty locating asteroids amongst the high number of background stars, or when the opposition region is not above about 1.5 airmasses.

Recent interest in large scale surveys of the sky for NEAs have promoted studies of their sky plane distribution (Bowell & Muinonen 1994) in order to determine where scanning is most profitable. The sky plane density of NEAs decreases with ecliptic latitude, while the increase in brightness of asteroids towards opposition enhances the number of NEAs in that direction. Large scale, wide field surveys plan to cover the sky many times during the dark period of each lunation

 0004-6256/96/111(2)/970/13/$6.00  

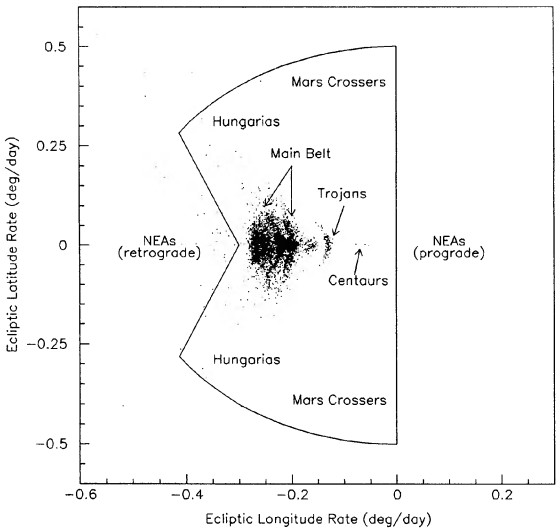


FIG. 1. Typical rates of motion and identification for asteroids found near opposition.

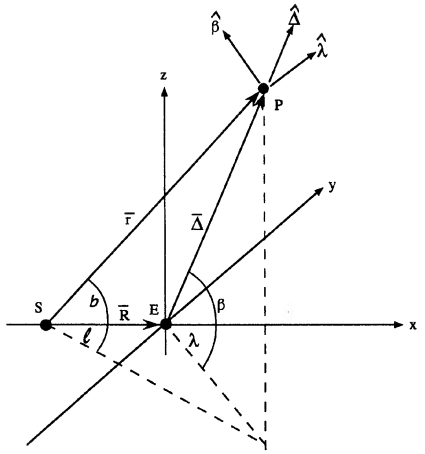


FIG. 2. Definition of vectors and angles.

and thereby repeatedly recover all asteroids in their scans within a couple weeks. Theoretically, this method will allow them to identify the same asteroids in successive passes, calculate good orbits, and identify those which are NEAs. Their proposed scanning technique provides them with some advantages over Spacewatch's current method but the practical development and implementation of their identification and matching software awaits testing.

Bowell & Muinonen (1994) used a model NEA distribution and examined their location on the sky plane by calculating the positions of all the asteroids as viewed from Earth at various times. Their study allowed them to reach several important general conclusions about the nature of future NEA survey programs. However, they were not concerned with the ability to identify the objects based on their rates of motion.

The apparent rates of motion of asteroids which will impact Earth within about 100 days has been studied by Hills & Leonard (1995). Ten days before impact the maximum geocentric proper motion is about 300 arcsec/day with a comparable reflex proper motion due to the Earth's rotation. Spacewatch's current method of motion detection can locate objects moving as slow as 150 arcsec/day and, by doubling the time between successive passes over a region, it is possible to halve the rate of motion of detectable objects. Many of the objects described in their paper are easily detected using the current Spacewatch configuration. If the combined proper and reflex motion produce NEAs moving at rates which are significantly different from other objects in the same field of view they may be flagged as interesting candidates by the Spacewatch observers.

The present paper develops an analytical measure of the probability that an object discovered at a specified location with respect to opposition, and with a given geocentric rate of motion, is a NEA. Discovery programs may then set a limit on the probability before deciding to follow it for a better orbit determination. The predicted NEA discoveries are examined as a function of ecliptic latitude and longitude with respect to opposition, confidence level for a positive identification, the magnitude limit of the detection system, and the absolute magnitude of the discovered NEAs. In all cases it is possible to determine the location on the plane of the sky which maximizes the probability of NEA detection by motion alone. Since this method relies on the instantaneous rates of motion of an asteroid it allows identification and almost immediate follow-up of faint objects. These fainter asteroids may be bright enough for detection in the large scale surveys during a single pass but may not remain above their detection threshold for a period of time sufficient to reacquire them and calculate orbits.

## 2. METHOD

### *2.1 Determination of the Geocentric Ecliptic Rates of Motion*

Let **r**, **R**, and **Δ** vectors be defined between the Sun ($S$), Earth ($E$), and another solar system object ($P$) as shown in Fig. 2, where **r**=**SP**, **R**=**SE**, and **Δ**=**EP**. Then define a right-handed Cartesian coordinate system with $\hat{x}$ (all variables with a hat are unit vectors) pointing towards the Vernal Equinox, and $\hat{z}$ in the direction of the North Ecliptic Pole. In order to view the object $P$ from the Earth, a telescope must be pointed in the direction $\hat{\Delta}$. Thus, $\mathbf{r}=\mathbf{R}+\mathbf{\Delta}=\mathbf{R}+\Delta\hat{\Delta}$, where $\Delta$ is the distance between the Earth and the object. If the pointing direction ($\hat{\Delta}$) is specified, then for every $\Delta$ there will be some set of $(a,e,i)$=(semimajor axis, eccentricity, inclination) for which it is dynamically possible to find an object at **Δ** (or, equivalently, **r**). In other words, only certain $(a,e,i)$ combinations can place an object at **r**. The range of allowed values is given by the following two equations:

$$a(1-e)\leqslant r\leqslant a(1+e),$$

$$\sin i\geqslant\frac{|r_z|}{r},$$

where $r_z$ is the $z$ component and $r$ is the magnitude of **r**. The first equation states that an object can only be found between perihelion and aphelion. The second equation represents the

fact that it is impossible to find an object with a heliocentric ecliptic latitude which is greater than the inclination of the orbit.

Given that an object resides at $\mathbf{r}$ and has orbital elements $(a,e,i)$, the speed $(v)$, and magnitude of the angular momentum $(h)$ are given by

$$v^2=\mu\left(\frac{2}{r}-\frac{1}{a}\right),$$

$$h^2=\mu a(1-e^2),$$

where $\mu=G\mathcal{M}_\odot$, $G$ is the Gravitational constant and $\mathcal{M}_\odot$ is the mass of the Sun.

In order to solve for the angular momentum vector ($\mathbf{h}$) it is necessary to determine the longitude of the ascending node ($\Omega$) which the orbit must have in order to place the object at $\mathbf{r}$. If $l$ and $b$ represent the heliocentric ecliptic longitude and latitude of the object, respectively, then

$$\tan l=\frac{r_y}{r_x},$$

$$\sin b=\frac{r_z}{r},$$

where $r_x$ and $r_y$ are the $x$ and $y$ components of $\mathbf{r}$, respectively. The ascending node for this object can then be determined from Moulton (1914)

$$o\equiv(l-\Omega)=\sin^{-1}\left(\frac{\tan b}{\tan i}\right)$$

leading to two possible solutions

$$\sin\Omega_{12}=\pm\sin(l\mp o),$$

$$\cos\Omega_{12}=\pm\cos(l\mp o),$$

where the "12" subscript on $\Omega$ indicates that it has two possible values: the "1" solution corresponding to the upper sign in each case, and the "2" designating the lower sign. For each of these two solutions there exists an angular momentum vector whose three components are given by

$$h_x=h\sin\Omega_{12}\sin i,$$

$$h_y=-h\cos\Omega_{12}\sin i,$$

$$h_z=h\cos i.$$

Using the fact that $\mathbf{h}=\mathbf{r}\times\mathbf{v}$, it is easy to show that

$$\mathbf{v}=\frac{\mathbf{r}(\mathbf{r}\cdot\mathbf{v})-\mathbf{r}\times\mathbf{h}}{r^2}$$

and squaring both sides of this equation and solving for $\mathbf{r}\cdot\mathbf{v}$ yields

$$\mathbf{v}=\frac{\pm\mathbf{r}\sqrt{r^2v^2-h^2}-\mathbf{r}\times\mathbf{h}}{r^2}.$$

The combination of the two possible values of $\Omega$ with both solutions for $\mathbf{r}\cdot\mathbf{v}$ yields four possible orbits which can place an object with $(a,e,i)$ at $(\mathbf{r},\boldsymbol{\Delta})$.

The relative velocity of the asteroid with respect to the Earth is then

$$\mathbf{v}_{\rm rel}=\mathbf{v}-\frac{d\mathbf{R}}{dt}.$$

Assuming the Earth is on a circular orbit, the magnitude of the Earth's velocity is $\sqrt{\mu}$. The angular rate vector with respect to the Earth is

$$\boldsymbol{\omega}=\frac{\mathbf{v}_{\rm rel}}{\Delta}$$

and the geocentric ecliptic rates of motion are then easily obtained by considering the projection of the angular rate vector onto the three unit vectors

$$\hat{\lambda}'=(-\sin\lambda',\cos\lambda',0), \tag{1a}$$

$$\hat{\beta}=(-\sin\beta\cos\lambda',-\sin\beta\sin\lambda',\cos\beta), \tag{1b}$$

$$\hat{\Delta}=(\cos\beta\cos\lambda',\cos\beta\sin\lambda',\sin\beta), \tag{1c}$$

where $\lambda'$ is the geocentric ecliptic longitude with respect to opposition ($\lambda'=\lambda-\lambda_{\rm oppn}$, and $\lambda_{\rm oppn}$ is the ecliptic longitude of opposition) and $\beta$ is the ecliptic latitude. These three vectors represent the geocentric directions of increasing ecliptic longitude, latitude and distance respectively. For objects which are not too close to the Earth the geocentric and topocentric rates of motion will be very similar. Thus, the rates of motion in each direction for a geocentric observer are

$$\dot{\lambda}'=\boldsymbol{\omega}\cdot\hat{\lambda}',$$

$$\dot{\beta}=\boldsymbol{\omega}\cdot\hat{\beta},$$

$$\dot{\Delta}=\boldsymbol{\omega}\cdot\boldsymbol{\Delta}.$$

It is not difficult to show that these expressions reduce to those derived by Bowell *et al.* (1990) at opposition assuming that the Earth is at $\mathbf{R}=(1,0,0)$:

$$\dot{\beta}=\pm\frac{\sqrt{\mu}}{r(r-1)}\sqrt{a(1-e^2)}\sin i,$$

$$\dot{\lambda}=\frac{\sqrt{\mu}}{r-1}\left[\frac{\sqrt{a(1-e^2)}}{r}\cos i-1\right].$$

It is slightly more time consuming to prove that these equations imply that the rate distribution for asteroids, $(\dot{\lambda}',\dot{\beta})$, will be mirror symmetric at any location with respect to the ecliptic. In other words, a plot of the rate distributions at $(\lambda',\beta)$ will be the mirror reflection about $\dot{\beta}=0°$/day of the rate distribution at $(\lambda',-\beta)$. Similarly, the rate distribution will be mirror symmetric about $\dot{\beta}=0°$/day under the transformation $\lambda'\rightarrow-\lambda'$. The longitude and latitude symmetries agree for the most part with conventional wisdom, but the origin of this effect relies on a wonderful correlation between the four possible orbital solutions. In general, an object with $\mathbf{v}$ at $(l,b)$ rotated in ecliptic longitude about the Sun to $(-l,b)$ will not have the same apparent geocentric rates of motion. However, the set of four possible orbits at both locations do agree with one another except for the mirror reflection about $\dot{\beta}=0°$/day.

### 2.2 Probability of Finding an Object in a Thin Geocentric Spherical Volume Element

In this section the probability is determined that an object with orbital elements $(a,e,i)$ will be found within a heliocentric bin at $\mathbf{r}=(r,l,b)$ of extent $(dr,dl,db)$. Since an object at perihelion is moving faster than at aphelion it is more likely to be found near aphelion than perihelion. Similarly, an object on an eccentric orbit is less likely to be found at a position near its longitude of perihelion. Finally, objects on inclined orbits spend a smaller fraction of their time, and are therefore less likely to be found, at small ecliptic latitudes.

The probability that an asteroid has specific values of $(a,e,i)$ is determined in the next section. In this analysis the distribution of the other three orbital elements $(M,\omega,\Omega)$ =(mean anomaly, argument of perihelion, longitude of the ascending node) are assumed to be independent and flat over their full ranges $(0,2\pi)$. In other words, the probability of finding an asteroid with mean anomaly in the range $M\rightarrow M+dM$, argument of perihelion in the range $\omega\rightarrow\omega+d\omega$, and ascending node in the range $\Omega\rightarrow\Omega+d\Omega$, is given by

$$P(M,\omega,\Omega)dMd\omega d\Omega = P(M)dM\ P(\omega)d\omega\ P(\Omega)d\Omega$$
$$= \frac{dM}{2\pi}\frac{d\omega}{2\pi}\frac{d\Omega}{2\pi}.$$

The heliocentric radial distance $(r)$ of an object depends only upon $(a,e,M)$ and therefore the probability that an object with $(a,e)$ will be found in the range $r\rightarrow r+dr$ is given by

$$P(r)dr = P(M)dM = P[M(r)]\frac{dM}{dr}dr = \frac{1}{2\pi}\frac{dM}{dr}dr.$$

Evaluating $dM/dr$, and recalling that an object will be in the desired range twice during an orbit (once while passing from perihelion to aphelion and again when returning), the radial probability density is given by

$$P(r) = \frac{1}{\pi}\frac{r}{a}\frac{1}{\sqrt{2ar-r^2+a^2(e^2-1)}}.$$

The expression for the probability of finding the object in a range of heliocentric ecliptic latitude may be derived starting from

$$\sin b = \sin i\ \sin[\omega+\nu(M)],$$

where $\nu$ is the true anomaly which depends upon $(e,M)$. Since the ecliptic latitude is independent of $\Omega$ the differential probability density is given by

$$dP = \frac{1}{4\pi^2}dMd\omega.$$

Letting $b(M,\omega)=\sin^{-1}\{\sin[\omega+\nu(M)]\ \sin i\}$, the probability density in ecliptic latitude is given by the expression

$$P(b) = \frac{1}{4\pi^2}\int_{-\pi}^{+\pi}dM\int_{-\pi}^{+\pi}d\omega\,\delta[b-b(M,\omega)].$$

Integrating over the argument of perihelion requires converting the argument of the delta function to one which is explicitly dependent on $\omega$ so that

$$P(b) = \frac{1}{4\pi^2}\int_{-\pi}^{+\pi}dM\int_{-\pi}^{+\pi}d\omega \times\sum_{i=1}^{2}\delta(\omega-\omega_i)\Big/\left|\frac{\partial[b-b(M,\omega)]}{\partial\omega}\right|_{\omega=\omega_i},$$

where the $\omega_i$ are the two zeros of the equation $b-b(M,\omega)=0$. Evaluation of this expression yields a probability density in ecliptic latitude of the form

$$P(b) = \frac{1}{\pi}\frac{\cos b}{\sqrt{\sin^2 i-\sin^2 b}}. \quad (3)$$

This equation is applicable to orbits with $i\neq 0$ and for $b<i$. For $i=0$ it should be obvious that $P(b)db=0$ unless the ecliptic latitude range $(b\rightarrow b+db)$ spans $b=\beta=0$ in which case $P(b)db=1$.

The expression for the probability density in heliocentric ecliptic longitude might be guessed without a detailed calculation but in the interest of completeness a few steps are given here. As for the ecliptic latitude calculation, the probability density in longitude is given by

$$P(l) = \frac{1}{8\pi^3}\int_{-\pi}^{+\pi}dM\int_{-\pi}^{+\pi}d\omega\int_{-\pi}^{+\pi}d\Omega\,\delta[l-l(\omega,M,\Omega)],$$

where

$$l(\omega,M,\Omega)=\Omega+\tan^{-1}\{\tan[\omega+\nu(M)]\cos i\}$$

and, unlike the cases in radial distance and ecliptic latitude, an object is only at a specific heliocentric longitude a single time during an orbit. Integrating this expression yields simply $P(l)=1/(2\pi)$.

The expressions for $P(r)$, $P(b)$, and $P(l)$ integrate to one over the allowed ranges in each variable, and the combined expression for the probability density of finding an object with $(a,e,i)$ in a heliocentric bin at $(r,l,b)$ is finally

$$P(a,e,i;r,l,b) = \frac{1}{2\pi^3}\frac{r}{a}\frac{1}{\sqrt{2ar-r^2+a^2(e^2-1)}}\frac{\cos b}{\sqrt{\sin^2 i-\sin^2 b}}.$$

The integration which follows requires a determination of the probability of finding an asteroid in a geocentric spherical volume element. The geocentric pointing vector of the telescope is given by Eq. (1c) and $\mathbf{\Delta}\equiv\Delta\hat{\Delta}$. Let the field of view (or of interest) have a dimension in each direction of $(d\lambda',d\beta)$.

The probability of finding an object with $(a,e,i)$ in a thin geocentric spherical element of dimensions $(d\Delta,d\lambda',d\beta)$ and location $(\Delta,\lambda',\beta)$ corresponding to a thin heliocentric spherical element of dimensions $(dr,dl,db)$ and location $(r,l,b)$ is given by

$$P(a,e,i;\Delta,\lambda',\beta)d\Delta d\lambda' d\beta = P(a,e,i;r,l,b)drdldb$$
$$= P(a,e,i;r,l,b)\times\left|\frac{\partial(r,l,b)}{\partial(\Delta,\lambda',\beta)}\right|d\Delta d\lambda' d\beta,$$

where the Jacobian of the heliocentric-geocentric transformation has been introduced. The geocentric probability density is immediately identified as

$$P(a,e,i;\Delta,\lambda',\beta)=P(a,e,i;r,l,b)\left|\frac{\partial(r,l,b)}{\partial(\Delta,\lambda',\beta)}\right|,$$

where $(r,l,b)$ are evaluated at $(\Delta,\lambda',\beta)$.

While the purpose of this derivation was to determine the probability that a new object is a NEA based upon its rates of motion given an $(a,e,i)$ distribution, work is in progress to use the method to determine the orbital bias and magnitude bias of an asteroid search program.

### *2.3 Model for the Orbit and Absolute Magnitude Distribution of Asteroids*

Let $P_g(a,e,i)dadedi$ be the probability that an asteroid which is a member of a group $g$ has orbital elements in the range $(a\rightarrow a+da,e\rightarrow e+de,i\rightarrow i+di)$. The probability density function $P_g(a,e,i)$ should be determined from a debiased distribution of orbital elements for all the asteroids of interest. The orbital distribution for each type of asteroid is determined independent of the total number of asteroids in the different classes so that

$$\int_a\int_e\int_i P_g(a,e,i)dadedi=1$$

and the number of asteroids in a class $g$ is determined by the unbiased distribution in absolute magnitude.

Let $n_g(H)dH$ be the number of asteroids of class $g$ in the absolute magnitude range $H\rightarrow H+dH$. Then the total number of asteroids brighter than $H'$ of class $g$ in the orbital element range $(a\rightarrow a+da,e\rightarrow e+de,i\rightarrow i+di)$ is given by

$$P_g(a,e,i)dadedi\int^{H'} n_g(H)dH.$$

Unfortunately, a debiased distribution of asteroid orbits suitably normalized between the various classes does not exist. Instead, this study considers five classes of asteroids as distinct groups: NEA, Mars Crossing (MC), Hungaria (HU), Main Belt (MB), and Trojan (TR). The experience of the Spacewatch surveys indicates that the MC and HU asteroids are most likely to cause confusion with a NEA identification and therefore deserve special consideration.

The unbiased $(a,e,i)$ distribution for the Main Belt ($2.1<a\leq 4.2$) was obtained by using the existing set of numbered asteroids (6160 asteroids as of 1995 March 29) and applying an absolute magnitude cut at $H=11.0$. This cut was motivated by Fig. 2 of Durda & Dermott (1995) which shows that relatively few of the asteroids discovered in the past forty years have $H<11$, implying that the known sample is almost complete to this absolute magnitude. The cut left 1371 asteroids in bins 0.2 AU wide in $a$, 0.1 wide in $e$ ($e\leq 0.9$), and 5.0° wide in $i$ ($i\leq 70$). The choice of bin size was motivated by the existing information for the NEAs as described below and was used for all five sets of asteroids.

The magnitude-frequency distribution for the bright ($H\leq 11$) Main Belt asteroids was determined from the same set of asteroids binned in 0.5 mag intervals. The data was fit to a distribution of the form

$$n(H)dH=(H-H_0)^{\alpha}dH \quad H\geq H_0$$
$$=0 \quad H<H_0.$$

This functional form provides a better fit to the data than the traditional $e^{mH+b}$ and the $H_0$ parameter is immediately identified as being representative of the brightest asteroid in the group. The integrated number of asteroids to an absolute magnitude $H$ is then simply

$$N(H)=\frac{(H-H_0)^{\alpha+1}}{\alpha+1}.$$

For the MB asteroids, the fit yielded $H_0=3.8\pm 0.1$ and $\alpha=3.33\pm 0.03$. In this and subsequent fits to the absolute magnitude distribution, the adopted value for $H_0$ is always one for which $\alpha$ was fixed at a reasonable value. For the MB sample $\alpha$ was fixed at 3.33 yielding $H_0=3.75\pm 0.03$.

The results of this study will be compared with the Spacewatch survey which can detect kilometer sized asteroids within the MB. Asteroids in this size range have absolute magnitudes of about 18.4 (averaged over C and S type asteroids using the albedos of Tholen & Barucci 1989). Since the MB asteroids form the largest number of Spacewatch detections, their magnitude–frequency relation must be treated specially when extended to the limiting absolute magnitude of the system.

The numbered asteroids show a distinct increase for $H>11$ above the extrapolation of the fit to the asteroids with $H<11$. This increase is confirmed by the Palomar Leiden Survey of Faint Minor Planets (van Houten *et al.* 1970) which is bias corrected through the entire MB in the range of about $10.5<H<15.0$. A fit to their data in this range yields $\alpha=3.81\pm 0.03$—quite different from the value obtained for the bright MB asteroids. Other than the two half-magnitude intervals between absolute magnitudes 12 and 13 (which were excluded in the fit) the data points agree well with the fit over the range. The value of $H_0$ in this $H$ range was chosen to ensure that at $H=11$ the two functions agreed exactly.

Extrapolating the MB magnitude-frequency relation to even fainter absolute magnitudes required the use of (as yet) unpublished but debiased data on the distribution of faint MB asteroids using Spacewatch data. For $H>14$ the data is fit well by an exponential function of the form $n(H)\propto 10^{0.6H}$ *and the proportionality constant was chosen so that at* $H=14$ the distribution agreed with that of the brighter asteroids. Table 1 summarizes the values for $H_0$ and $\alpha$ for the five groups of asteroids considered in this section.

While it is generally accepted that the known sample of Main Belt asteroids is complete to $H\sim 11$ there has been no consideration as yet of the completeness of the Mars Crossing and Hungaria asteroids. Since the Hungaria asteroids ($1.78\leq a\leq 2.00$, $e\leq 0.18$, $16\leq i\leq 34$, as defined by Zellner *et al.* 1985) occupy a relatively small volume of the $(a,e,i)$ space, it was assumed that the strong bias observed through

TABLE 1. Parameters of the magnitude–frequency relation $n(H)dH=(H-H_0)^{\alpha}$ for the five different classes of asteroids considered. In each case the value of $\alpha$ was fixed at the value specified here after performing a fit where it was allowed to float.

| Asteroid Type | Range of Fit | $H_o$ | $\alpha$ |
|---|---|---|---|
| NEA | $12.0 \leq H \leq 13.5$ | 11.5 ±0.1 | 3.33 |
| Mars Crosser | $10.5 \leq H \leq 12.5$ | 9.85±0.09 | 3.33 |
| Hungaria | $11.0 \leq H \leq 13.5$ | 10.46±0.08 | 3.33 |
| Main Belt | $5.0 \leq H \leq 11.0$ | 3.75±0.03 | 3.33 |
| | $11.0 \leq H \leq 14.0$ | | 3.81 |
| | $14.0 \leq H \leq 19.0$ | | 0.6[a] |
| Trojan | $7.0 \leq H \leq 14.0$ | 6.26±0.07 | 3.70 |

[a]In this range $n(H) \propto 10^{\alpha H}$

the Main Belt would not be as dramatic for these asteroids. Therefore, all the known Hungaria asteroids (59) were used to determine the orbital distribution in $(a,e,i)$ for this class. The same arguments about a relatively unbiased distribution for the Hungarias can not be applied to the Mars Crossing asteroids [$1.3<a(1-e)\leq 1.666$ AU, as defined by Zellner *et al.* 1985] since they may occupy an expansive region of the $(a,e,i)$ space. However, there are so few MC asteroids that all known members (149) were included in defining their orbital distribution.

The magnitude-frequency distribution for MC and HU asteroids has not been published. Motivated by the same argument used for MB asteroids, it was assumed that most of the brighter members of these two families are known and therefore the magnitude–frequency relation in the first few magnitude bins is indicative of the group. The MC and HU asteroid's absolute magnitude distributions in 0.5 mag. bins were fit in the ranges $10.5\leq H\leq 12.5$ and $11.0\leq H\leq 13.5$, respectively. The values of $\alpha$ so determined are consistent with the value for the brighter MB asteroids of 3.33. The $H$ distribution was then refit in the same range with $\alpha=3.33$ allowing only $H_0$ to float.

The Trojan asteroids ($5.05\leq a\leq 5.40$, Zellner *et al.* 1985) are not expected to cause much confusion with a NEA identification based upon rates of motion since they move even slower than MB asteroids. They are included in this study for completeness and because a small fraction of observable NEAs can have rates of motion consistent with an interpretation of a Trojan origin. Once again, the argument used to justify using all HU asteroids is applied equally well to the Trojan's orbit distribution. There are 117 numbered Trojans in the list used here. However, the Trojans are only present in an observation region when it encompasses one of the L4 or L5 groups. Unlike the other four groups, the Trojan asteroids are not randomly distributed in their mean anomaly at any epoch since they maintain the appropriate separation from Jupiter. Removing the Trojans from consideration only increases the probability of identification of asteroids as NEAs, so they are included in this study as a worst-case scenario.

The magnitude-frequency relation of the Trojans has been considered by Shoemaker *et al.* (1989). They argued that the L4 Trojan sample at the time was complete to $B(1,0)=9.75$ (corresponding to $H\sim 8.75$). A fit to the standard functional form used here for the absolute magnitude of all the numbered Trojans in the range $7.0\leq H\leq 9.0$ yields $\alpha=3.7\pm 0.2$. In order to be consistent with the fitting technique used for the other classes of asteroids, $\alpha$ was fixed at 3.7 in a subsequent fit yielding the results shown in Table 1. This value of $\alpha$ is consistent with the value derived for the (as yet) unpublished debiased magnitude-frequency distribution for Trojan asteroids using Spacewatch detections in the range $9.0\leq H\leq 14.0$. Thus, a single value of $\alpha$ fits the distribution of Trojans over a change in diameter by a factor of about 25. In the L4 swarm alone Shoemaker *et al.* (1989) expect 1000 ±200 asteroids to $B(1,0)=14$ ($H\sim 13$). The total expected number of Trojans to $H=13$ using the functional form and fit given here yields about 1700 asteroids for the combined L4 and L5 swarm, consistent with the Shoemaker expectation.

The debiased differential orbital distribution of the NEAs was derived from that published by Rabinowitz (1994) for asteroids greater than about one kilometer in diameter. The integral $P(a,e)$ and $P(i)$ he presents (his Tables III and IV) are not in the standard form of an integral probability but may still be inverted to provide the differential distribution required for this study.

Rabinowitz *et al.* (1994) estimate that the known population of NEAs brighter than $H=13.5$ is complete. Once again, an estimate of the magnitude–frequency relation for the NEAs is obtained by fitting the known absolute magnitude distribution in the range $12.0\leq H\leq 13.5$ in 0.5 magnitude bins. A fit with floating $\alpha$ yields a value consistent with $\alpha_{MB}=3.33$ justifying a subsequent fit with fixed $\alpha=\alpha_{MB}$. The expected total number of NEAs larger than one kilometer diameter using this fit is about 1000, consistent with recent estimates of about 1500 NEAs in this size range (Rabinowitz *et al.* 1994).

The method described above yields a debiased differential distribution in $(a,e)$ space integrated over $i$ for asteroids larger than one kilometer in diameter as shown in Fig. 3(a). For the purpose of integrating the final set of equations given below, an entire bin in the $(a,e)$ space was assigned to the type of asteroid represented by the center of the bin. The NEAs are well distributed throughout the space below about 3 AU in semimajor axis. Due to the requirement that the center of a bin defines the type of asteroid for the entire bin, the Hungarias appear to occupy only a single bin in $(a,e)$. In reality, the Hungarias overlap in parts of two bins with the Mars Crossing asteroids.

Similarly, Fig. 3(b) shows the debiased differential distributions in inclination integrated over $(a,e)$ for each of the five classes of asteroids. It shows that the NEAs possess a tail to very high inclinations as well as a peak in the range $35°<i\leq 40°$. It is not possible to determine the statistical significance of this structure given the information provided by Rabinowitz (1994). The Mars Crossing asteroids are the group for which the debiasing procedures used here are least applicable. One half of all the known MC asteroids appear in the prominent peak in the range $20°<i\leq 30°$, very near the same region of inclinations occupied by the Hungarias. However, Fig. 3(a) shows that only 15% of the MC asteroids in

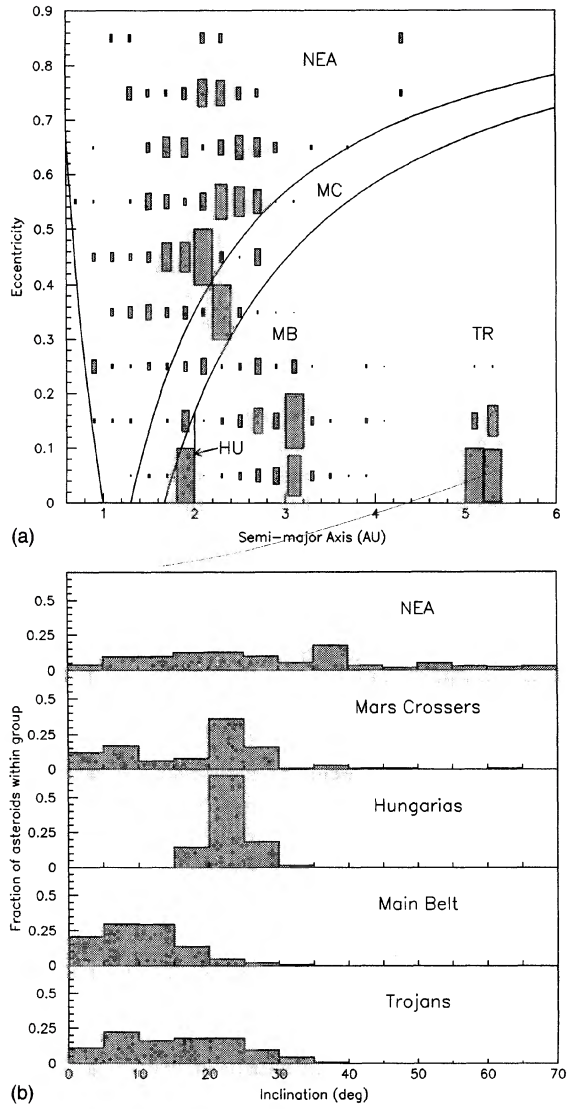


FIG. 3. Debiased differential distribution for asteroids greater than 1 km in diameter used in this study. The NEA distribution was derived from Rabinowitz (1994) and the distribution for all the other asteroids was determined from the set of numbered asteroids: (a) The fractional distribution of asteroids in $(a,e)$ within each group is indicated by the size of the boxes. The curves delineate the different groups of asteroids; (b) The fractional distribution in inclination for the five groups of asteroids considered in this study.

the peak occur in the range of $(a,e)$ defining the Hungarias, while one-half of them appear to be a high-eccentricity type of Phocaea with eccentricity in the range $0.29 \leq e \leq 0.40$. The Hungarias occupy a limited but relatively high region in inclination space. It is their high inclination and presence on the inside of the Main Belt which may cause confusion with the NEAs. The last histogram in Fig. 3(b) illustrates the well-known observation that the Trojans have a higher mean inclination than the MB asteroids.

While every effort has been made to ensure that the model asteroid distribution accurately reflects the actual orbital element distribution, it must be remembered in the ensuing discussion that there are large extrapolations of the known populations to the faint magnitude limits of detection systems like Spacewatch. This point is well illustrated by the difficulties of extending the MB magnitude–frequency relation beyond the completeness limit of the numbered asteroids. A simple extrapolation of the known distribution to the magnitude limit of Spacewatch yields far too few observable asteroids per square degree on the sky. It is quite probable that the extrapolation of the relation for the other sets of asteroids is equally problematic.

For instance, Rabinowitz *et al.* (1993) hold that there exists a belt of small NEAs with orbital elements similar to the Earth's. Further, Rabinowitz (1994) claims that there is a strong enhancement in the number of NEAs per absolute magnitude interval for the small objects (<100 m diameter). These effects would enhance the number of observable NEAs in this simulation. The problem is avoided by only considering the detection of NEAs greater than 100 m in diameter. These observations may be real or an artifact of the debiasing procedure, but they are probably the best available in the literature and are used here subject to the aforementioned caveats.

### *2.4 Determining the Probability that an Asteroid is a NEA Based Upon its Rates of Motion*

The number of visible objects ($\eta$) of type $g$ with rates in the range $(\dot{\lambda}' \rightarrow \dot{\lambda}' + d\dot{\lambda}', \dot{\beta} \rightarrow \dot{\beta} + d\dot{\beta})$ when examining a region of extent $(d\lambda', d\beta)$ in the direction $\hat{\Delta}$ and using a detection system with limiting magnitude $V_{\rm lim}$ is given by

$$\eta_g(\lambda',\beta;\dot{\lambda}',\dot{\beta})d\lambda'\, d\beta\, d\dot{\lambda}' d\dot{\beta}$$

$$= \left| \int_0^\infty d\Delta \int da \int de \int di\; P_g(a,e,i)\; P(a,e,i;\Delta,\lambda',\beta) \right.$$

$$\left. \times d\Delta\; d\lambda'\; d\beta \int^{m(H)=V_{\rm lim}} dH\; n_g(H) \right|_{\substack{(\lambda \rightarrow \lambda + d\lambda, \beta \rightarrow \beta + d\beta) \\ (\dot{\lambda} \rightarrow \dot{\lambda} + d\dot{\lambda}, \dot{\beta} \rightarrow \dot{\beta} + d\dot{\beta})}} .$$

The condition on the integral requires that the $(\Delta,a,e,i)$ combination generates an object in the range of interest in both sky plane location and rates of motion. The limit on the integral over the absolute magnitude $[m(H) = V_{\rm lim}]$ specifies the value of $H$ at $(r,\Delta)$ which produces an object with an apparent visual magnitude at the limit of the system. This study does not take into account the decrease in apparent visual magnitude per unit imaging area with the rate of motion of the object. The apparent visual magnitude $m$ of an object with absolute magnitude $H$ was determined according to the IAU's Two-Parameter Magnitude System for Asteroids (Bowell *et al.* 1989) using a slope parameter of 0.15. Each of the integrals in this equation need only be evaluated over the range for which the two probability functions within the integrand are nonzero.

The probability $P(g)$ that an asteroid found in the direction $\hat{\Delta}$, with extent $(d\lambda', d\beta)$, and rates of motion in the range $(\dot{\lambda}' \rightarrow \dot{\lambda}' + d\dot{\lambda}', \dot{\beta} \rightarrow \dot{\beta} + d\dot{\beta})$ is an asteroid of type $g$ is given by

$$P(g)(\lambda',\beta;\dot{\lambda}',\dot{\beta}) = \frac{\eta_g(\lambda',\beta;\dot{\lambda}',\dot{\beta})}{\Sigma_{g'}\ \eta_{g'}(\lambda',\beta;\dot{\lambda}',\dot{\beta})}.$$

Thus, at any location in the sky, it is possible to define the probability that a newly discovered object is a NEA based upon the contemporary debiased distribution of asteroid orbits. Defining a cut on the probability ($P_{\rm cut}$) that an object is a NEA, it is possible to determine the most efficient location for detecting NEAs on the sky plane based on their rates of motion.

Finally, the number of NEAs distinguished by their rates of motion within $(\lambda' \rightarrow \lambda' + d\lambda', \beta \rightarrow \beta + d\beta)$ is determined by integrating $\eta_{\rm NEA}$ for that location over the $(\dot{\lambda}',\dot{\beta})$ space for $P({\rm NEA}) \geq P_{\rm cut}$:

$$N_{\rm NEA}(\lambda',\beta)\ d\lambda' d\beta = d\lambda' d\beta \left| \int d\dot{\lambda}' \int d\dot{\beta}\ \eta_{\rm NEA}(\lambda',\beta;\dot{\lambda}',\dot{\beta}) \right|_{P({\rm NEA}) \geq P_{\rm cut}}.$$

## 3. RESULTS

The integrations were carried out on a grid spacing of $2° \times 2°$ in ecliptic latitude and longitude with respect to opposition with $(d\lambda', d\beta) = (1°, 1°)$. At each location the $(\dot{\lambda}',\dot{\beta})$ space was divided into (160,240) bins in the ranges $-2°/{\rm day} \leq \dot{\lambda} \leq +2°/{\rm day}$ and $-3°/{\rm day} \leq \dot{\beta} \leq +3°/{\rm day}$ yielding a resolution of 0.025°/day. A separate counter was used to keep track of when the calculation produced an object whose rates of motion fell outside these ranges. Changing the limits on the range in rates or binning in $(\dot{\lambda}',\dot{\beta})$ has an insignificant effect on the results. The step sizes in $(a,e,i)$ were (0.05 AU, 0.025, 1.0°) and the integration over $\Delta$ was in the range 0.01 AU to a heliocentric distance of 6.0 AU in steps of 0.01 AU. In order to avoid singularities for $i=0$ in Eq. (3) the minimum allowed inclination was set at one-half the step size in $i$.

The particular step values were chosen based upon their effect on the total integration time, the memory limitations of the computer, and resolution of the output. A few longer integrations, using step sizes which required more than 300 times the computing time, and over 20 times the resolution in the $(\dot{\lambda}',\dot{\beta})$ space, indicate that the solutions presented here are stable. In order to allow a comparison with the simulations of Bowell & Muinonen (1994) the main integration was carried out requiring that the discovered NEAs have $H \leq 19.88$ corresponding roughly to their lower limit of 500 m on the diameter of NEAs.

Figure 4(a) shows the distribution of NEA identification probability in $(\dot{\lambda}',\dot{\beta})$ space for objects at opposition. Confidence level (C.L.) contours are drawn at 10%, 50%, and 90% corresponding to false:real detection ratios at roughly the 10:1, 1:1, and 1:10 level. The region outlined by the thick line is the same as in Fig. 1, corresponding to the rates typically avoided by the Spacewatch observers at opposition. This calculation agrees very well with the boundary of the interesting NEA rates on the left side of the Spacewatch zone and is almost superposed on the 50% NEA probability curve. There is also very good agreement on the right side of this zone at the 50% C.L. The spur which shows <90% probability for objects with very small latitudinal rates of motion and positive rates of longitudinal motion is an artifact due to the low inclination cut off in the integration.

Due to the relatively high inclination distribution of the Mars Crossing and Hungaria asteroids, they can display fast rates of motion in ecliptic latitude extending much further than the region typically avoided by Spacewatch observers. The distribution displays a characteristic butterfly pattern and is a mirror reflection about an ecliptic latitude rate of 0°/day as expected.

The four plots in Fig. 4 have been smoothed at one ninth the resolution of the original integration in order to reduce the raggedness of the curves. The residual raggedness is due to a variety of factors—mean motion and secular resonances, incompletion of the debiased orbital distributions, and the step size used in the integrations.

Figures 4(b)–4(d) show the same probability contours at $(\lambda',\beta)$ of (+45°,0°), (+45°,+20°), and (+45°,−20°), respectively. The shape of the C.L. contours change markedly from those at opposition. On the ecliptic, but removed from opposition, the contours appear to widen in longitudinal rate, and moving away from the ecliptic the rate plots seem to rotate about $(\dot{\lambda}',\dot{\beta}) = (0°,0°)$/day. As expected, the contour distributions are mirror symmetric about $\dot{\beta}=0°$/day for $\beta = \pm 20°$. The spreading of the rate distribution for all asteroids increases the confusion with the NEAs.

These figures allow a detection program to quantify the NEA identification probability for any asteroid using a contemporary debiased distribution of asteroid orbits. This ability is important to the debiasing of the program's discoveries to eliminate the subjective question of whether or not to follow an object on subsequent nights. A difference in judgement for discarding NEA candidates from observer to observer, or even from night to night by a single observer, will affect the bias of the observations.

Figures 4(a)–4(d) illustrate the usefulness of this technique for NEA surveys in terms of quantifying and selecting asteroids which are potentially NEAs. At the same time, these calculations provide a wealth of data useful for planning asteroid or NEA surveys and may be compared to the data obtained with the Spacewatch detector system which has a limiting magnitude of about 21.

Figure 5 shows contours of the sky plane density of asteroids (per sq. deg.) in ecliptic latitude and longitude relative to opposition. The integration predicts about 30 asteroids/sq. deg. at opposition. This agrees well with the actual number detected by Spacewatch of about 20 per sq. deg. after taking into account the mean efficiency of asteroid detection (about 65%). Notice that the sky plane density of asteroids decreases faster out of the plane of ecliptic than it does in the direction of increasing longitude.

The calculated sky plane density of all NEAs with absolute magnitudes less than 19.88 is shown in Fig. 6(a). At opposition there should be about 0.013 NEAs per sq. deg. to limiting visual magnitude 21, implying that about 77 sq. deg. of sky need to be scanned to ensure a NEA detection of this size or larger. These numbers agree very well with those

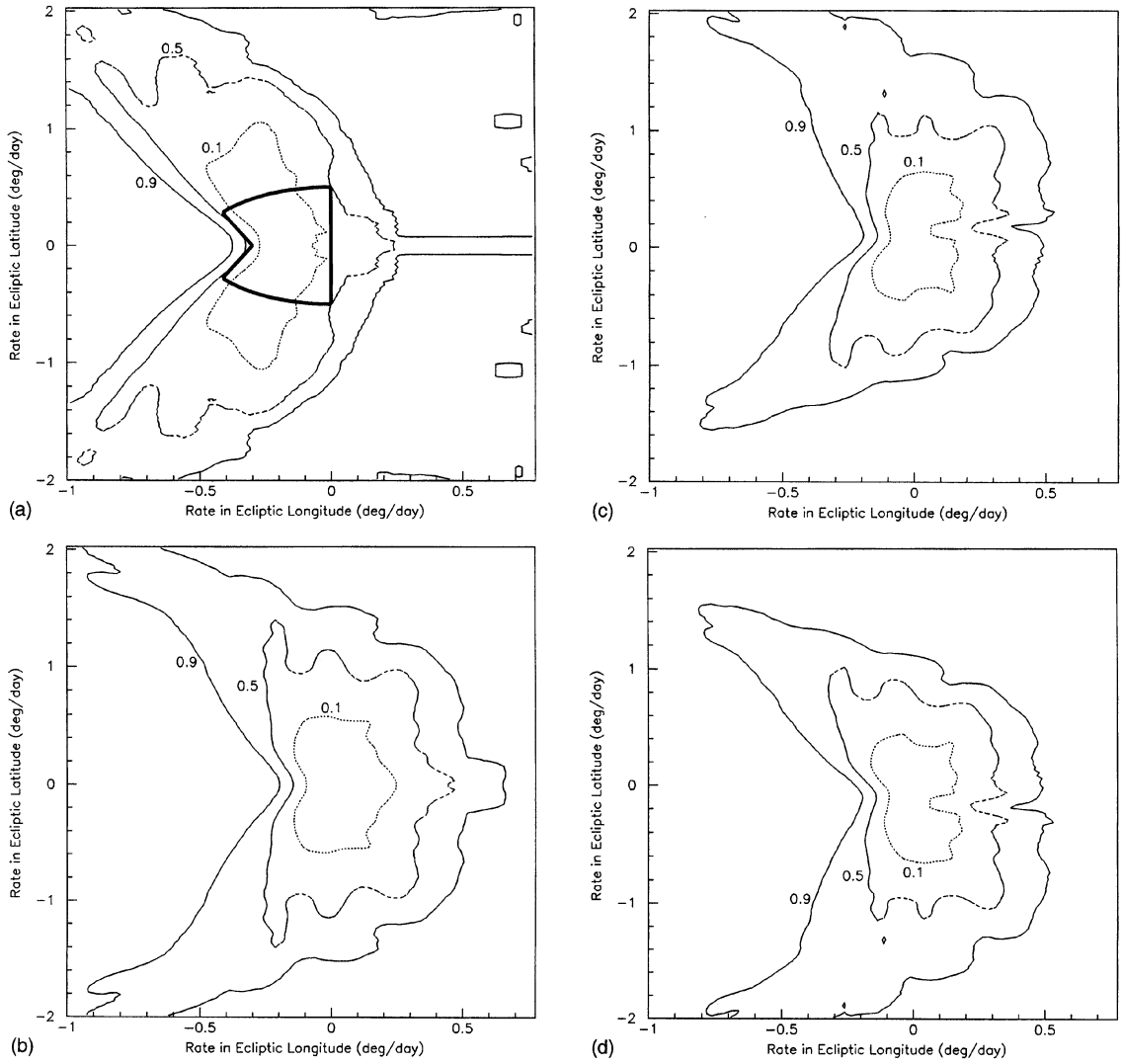


FIG. 4. Confidence level contours for detection of NEAs based on their rates of motion in the $(\dot{\lambda}', \dot{\beta})$ plane for a system with detection limit $V_{\rm lim}=21$ and for asteroids with $H \leq 19.88$ (corresponding to diameters greater than about 500 m). The contour levels indicate that any asteroid outside of the contour has greater than the contour probability of being a NEA. Contours are drawn at the 10%, 50%, and 90% confidence level corresponding roughly to false detections at the 10:1, 1:1, and 1:10 level: (a) C.L. curves for NEA motion vectors at opposition. The region outlined by the superposed dark curve is typically avoided by Spacewatch observers; (b) C.L. curves for NEAs 45° from opposition in longitude and on the ecliptic; (c) C.L. curves for NEAs 45° from opposition in longitude, and at an ecliptic latitude of +20°; (d) C.L. curves for NEAs 45° from opposition in longitude, and at an ecliptic latitude of −20°.

from Bowell & Muinonen (1994). The number density of the NEAs falls much more slowly with latitude than the density of non-NEAs (Fig. 5). This fact might lead to the conclusion that it is more effective to scan at high ecliptic latitudes than near the ecliptic. The statement is true for NEA detection programs which rely on rates of motion to distinguish asteroids, and which would otherwise be swamped by the total number of detections and measurements necessary to determine the rates for all the asteroids in the field of view close to the ecliptic. The real-time detection routines of Spacewatch are capable of handling the data acquisition and analysis for all the stars and asteroids in the field of view as long as the star density is not too great. This limits detection to galactic latitudes of more than about 25°.

Note that the sky plane density of NEAs begins to increase along the ecliptic more than about 30° from opposition due to a couple of factors. The volume of NEA space increases as the search area moves away from opposition, and the apparent brightness of an asteroid increases with phase angle (the angle between the Sun and Earth as viewed from the asteroid) at a fixed geocentric distance.

Figure 6(b) is most applicable to programs like Spacewatch. It shows the sky plane density in number of *detectable* NEAs per square degree as the search area moves away from opposition. A detectable NEA in this context is one which displays rates of motion which distinguish it from other asteroids at the 90% confidence level. Clearly, the best place to search for NEAs in this manner is at opposition where about 120 sq. deg. of sky must be searched to ensure a NEA detection.

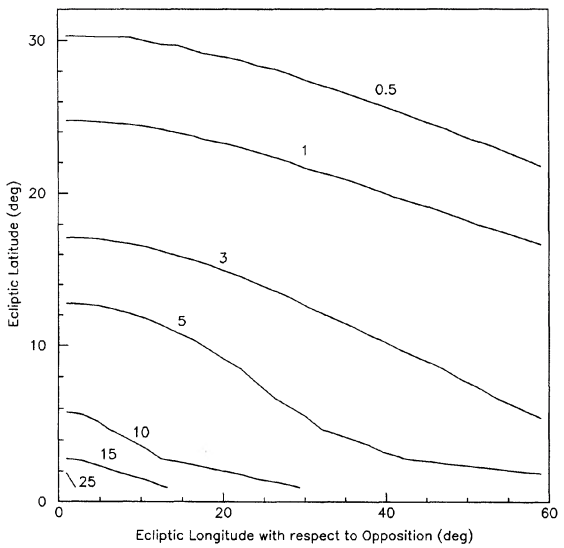


FIG. 5. Number of non-Near Earth asteroids per square degree to $V_{\rm lim}=21$ as a function of ecliptic latitude and longitude with respect to opposition.

The results displayed on Fig. 6(b) may be compared to the Spacewatch search which has discovered a total (as of 1995 May 28) of 97 NEAs of which about half are larger than 500 m in diameter. These NEAs were culled from the total sample of about 120 000 asteroids based upon their rates of motion, implying a ratio of all asteroids to larger NEAs of about 2400:1. A representative ratio predicted from these calculations is obtained from Figs. 5 and 6(b) at about 6° latitude and 10° in longitude yielding a ratio of about 1550:1. The predicted and observed ratios are in remarkable agreement, especially considering the facts that Spacewatch observers have not been using a quantitative measure of NEA identification to select follow up candidates, the lack of debiased orbital and magnitude information for the various asteroid classes, and the efficiency of the Spacewatch detection system.

Hypothetical detection systems which might have difficulty dealing with a large number of asteroids in the field of view could consider Fig. 6(c) which shows the fraction of all asteroids which are NEAs on the sky plane. At opposition, and to magnitude 21 for NEAs >500 m diameters, the NEAs make up a very small fraction of the total number of objects found. However, at 25° ecliptic latitude and 55° longitude from opposition, one in a hundred asteroids is a NEA—of course, finding 100 asteroids this far from opposition would take a long time. The same reasoning applies when forced to observe away from high-density star regions near the Milky Way.

The fraction of observable NEAs which are detectable by motion at the 90% C.L. is shown in Fig. 6(d). Even though the sky plane density of NEAs increases beyond 30° longitude from opposition, the fraction of NEAs distinguishable by their rates of motion continues to decrease.

The probability of finding a NEA per sq. deg. is, of course, dependent on the limiting magnitude of the detection system. Figure 7(a) shows how the probability per square degree of detecting a NEA by motion ($H\leq 19.88$) varies as a function of the limiting magnitude of the system and ecliptic longitude with respect to opposition along the ecliptic. Once again, this calculation does not take into account the decrease in apparent magnitude per unit area on the image due to trailing of the object. A roughly sixfold decrease in the sensitivity of the detection system ($V_{\rm limit}=19$) would correspond to a decrease in detectable NEAs by a factor of less than three at opposition. Similarly, increasing the magnitude limit to 23 yields about 1.6 times more NEA per square degree.

The NEA detection probability decreases monotonically with longitude from opposition for the detection systems with limiting magnitudes of 19 and 21 but increases to a local maximum for $V_{\rm lim}=23$. This effect is due to the interplay between the total number of observable NEAs as shown in Fig. 6(a), the increase in the total number of asteroids with absolute magnitude, the increase in volume searched as the detection region moves away from opposition, and the dependence of the apparent magnitude on the phase angle and distance of the asteroid. Since these calculations reflect detection of asteroids >500 m in diameter, it raises the prospect that efficient detection of larger NEAs with large telescopes might best be accomplished relatively far from opposition.

Detecting asteroids of $H\leq 19.88$ is of interest because the results allow comparison with other studies and because this size range of asteroids pose a real hazard to the safety of the Earth. Increasing the minimum detected asteroid size requirement to one kilometer corresponds to $H\sim 18.37$ and an increase of almost an order of magnitude in the energy of the impacting asteroid. Decreasing the size limit to only 100 m ($H\sim 23.37$) reduces their danger while increasing the frequency of impact of objects within the size range. They pose a regional threat and are interesting from the scientific viewpoint of their origin, evolution and makeup. Figure 7(b) shows how the detection probability of NEAs varies as a function of the limit on the absolute magnitude of the detected objects and as a function of ecliptic longitude with respect to opposition. Decreasing the absolute magnitude by five merely doubles the number of detectable asteroids at opposition. Smaller and fainter objects must be closer to the Earth in order to be observable. This means that they are moving faster and spend less time in the search volume which itself decreases as they approach the Earth.

The NEA detection probability per sq. deg. is not particularly sensitive to the confidence level of the NEA identification using this technique. Figure 7(c) shows the variation of this parameter as a function of ecliptic longitude with respect to opposition and for three representative values of the probability cut. Decreasing the probability cut from 0.9, where only 1 in 10 NEA candidates will turn out to be false, to 0.5 where every other candidate will not be an NEA, increases the probability of detecting a NEA by only about 10% at opposition. This is due to the relatively sharp change in NEA probability where the NEA density is highest in the $(\lambda',\beta)$ plots [where $\beta\sim 0$ and $\dot{\lambda}'<-0.3°$/day in Figs. 4(a)–4(d)] and the fact that the density of available NEAs is small where the probability contours change slowly. In principle, these results imply that a NEA detection program can tune

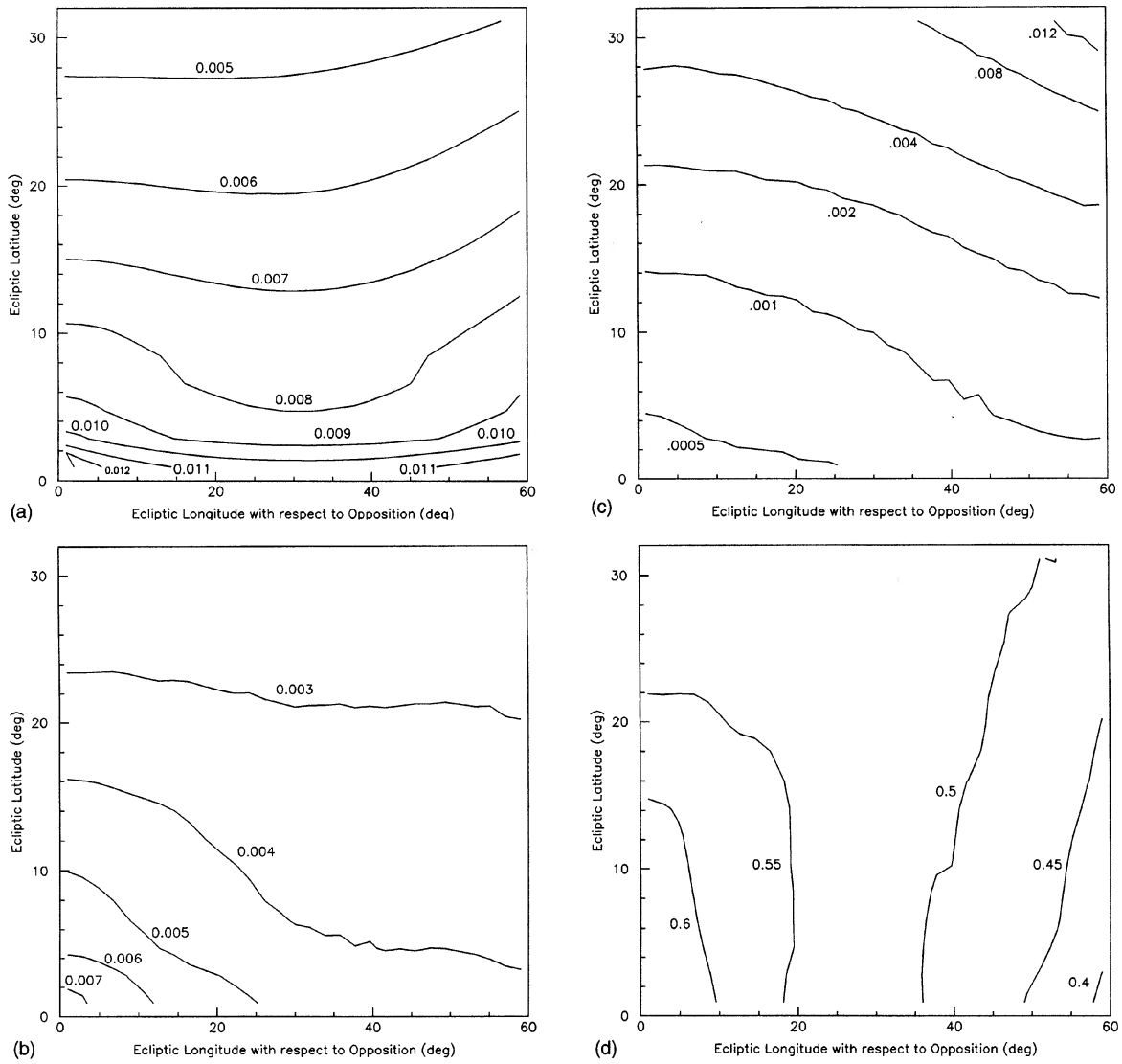


FIG. 6. (a) Number of NEAs with $H \leq 19.88$ per square degree to $V_{\rm lim}=21$ as a function of ecliptic latitude and longitude with respect to opposition; (b) As in (a) but for *detectable* NEAs as defined in the text; (c) The fraction of *all* asteroids which are *detectable* NEAs with $H \leq 19.88$ per square degree to $V_{\rm lim}=21$; (d) As in (c) but the fraction of detectable to total NEAs.

the false detections to a value which maximizes their detection rate after taking into account the time required for follow-up activities.

Ninety degrees from opposition, in the direction of the Earth's motion, where Hills & Leonard (1995) predict very small rates of geocentric proper motion for asteroids which will impact in ten days, most of the visible MB asteroids are moving prograde at about 12 arcmin/day and very few have rates of motion <5 arcmin/day. Any object whose motion is detectable and moving very slowly (recall that Spacewatch can find objects moving at ~2 arcmin/day) would be a candidate for a likely NEA and possible impactor. Since they derive that the reflex motion of these asteroids will be comparable to the maximum geocentric proper motion, it is likely that many of these impending impactors can be detected by a system similar to Spacewatch using rates of motion for identification.

Some comparison has already been made between the predictions of this calculation and the Spacewatch results but the litmus test should be the utility of the integrations and probability levels for a search program. Figure 8 shows the calculated probability of a NEA identification for 100 Spacewatch objects (a few of which were accidentally recovered, or were already known NEAs) at the time of discovery. The heavily shaded portion of the histogram is most applicable here since these objects have an absolute magnitude brighter than 19.88. For the brighter NEAs, and even more so for all the objects, there is a large spike in the last bin of probability.

Twenty-four of the 37 objects with $H \leq 19.88$ had a NEA probability >90% at the time of discovery according to these calculations. Six Spacewatch NEAs had a discovery probability calculated with this method of less than 50%. Three of these objects were found near opposition and had very low rates in ecliptic latitude while their longitudinal rates

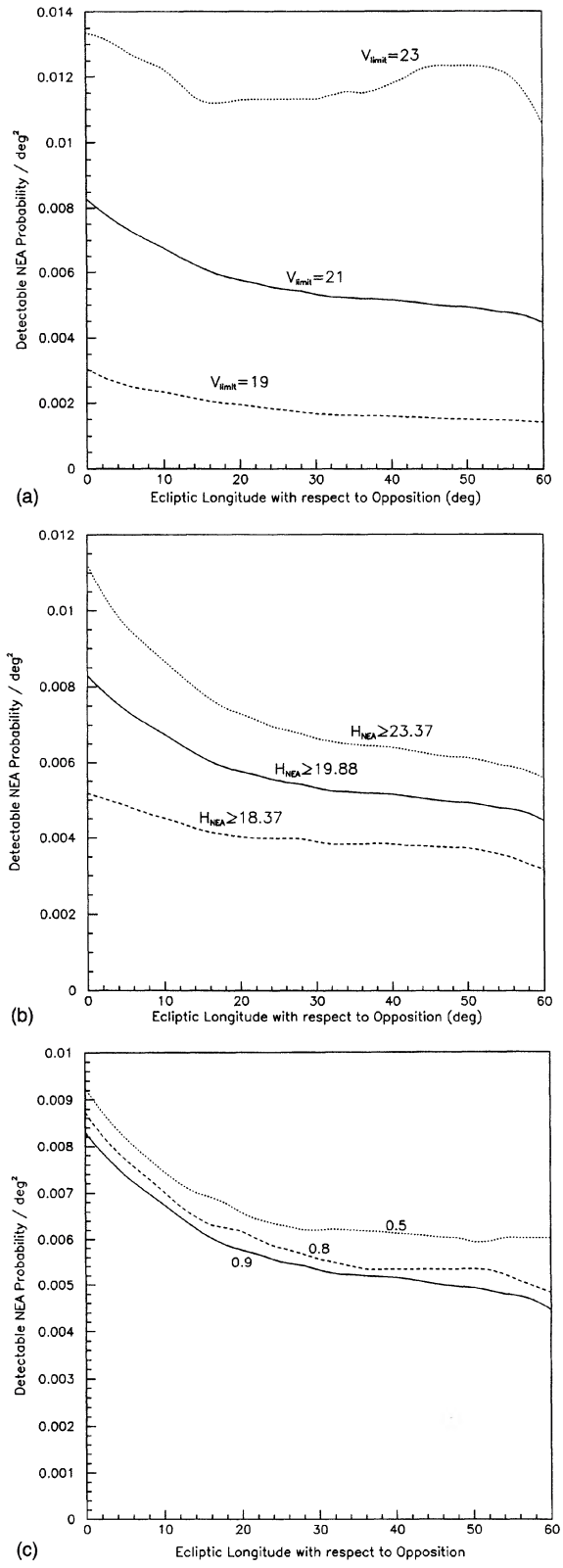


FIG. 7. The probability of detecting a NEA per square degree based only on its rates motion as a function of ecliptic longitude from opposition for: (a) three values of the system limiting magnitude; (b) three values of the limiting absolute magnitude of detected asteroids and; (c) three values of the confidence level cut on a NEA identification.

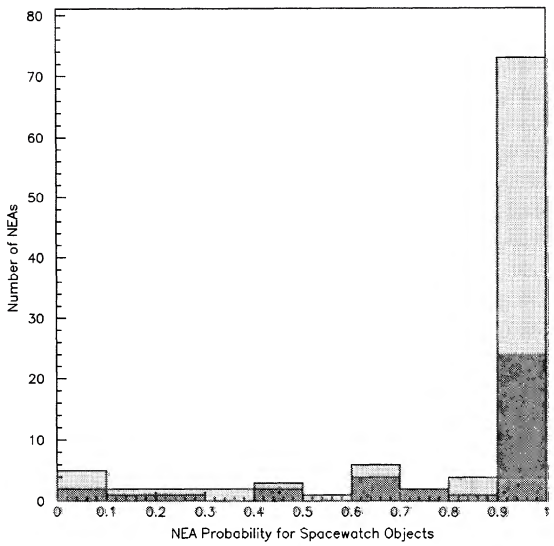


FIG. 8. The calculated probability for 100 NEAs detected by Spacewatch. The heavily shaded region corresponds to those NEAs with $H \leq 19.88$.

place them to the left of the "$V$" in Fig. 1. This is precisely the region where the probability contours are changing rapidly and the calculation is most sensitive to the orbital and absolute magnitude distributions for the various asteroids. It is also interesting to note that all three of these discoveries took place at the outset of the Spacewatch program when the false NEA identification rate was greatest. Allowing a lower probability for NEA candidates would increase the discovery rate. The other three of the six asteroids with less than 50% probability were discovered relatively far from opposition, about 21°, 39°, and 72°. Spacewatch observers are forced into scanning far from opposition when it is low in the sky and when the density of stars in the Milky Way interferes with the detection routine's capability. Under these circumstances the total rate of asteroid detections (and NEA detections) decreases dramatically and the observers cannot rely strongly on their experience gained mostly near opposition. It is not surprising that the NEA probability also drops for asteroids found under these conditions.

Accurate records are not kept of the number of false detections made at Spacewatch, but roughly 240 asteroids have been followed in order to make positive identifications of 97 NEAs. This ratio corresponds to a NEA probability required by an average Spacewatch observer of about 40%, consistent with Fig. 8. In the beginning of the program this number rose quickly from 20% to 30%.

## 4. CONCLUSIONS

The debiasing of Spacewatch data (and of other similar programs) is a difficult process subject to many considerations. Adopting a quantitative measure of the NEA probability as outlined here will increase the effectiveness of the discovery programs and benefit the analysis. The efficiency of the system may be measured as a function of the magnitude and rates of motion of the asteroid, but it may also depend on factors such as the local star density in an image

and the subjective choice of which NEA candidates to follow. Thus, in order to maximize the efficiency of a NEA discovery program, and to reduce the problems inherent in the debiasing of the data, existing and future detection programs which rely on the rates of motion for identification should consider adopting a procedure such as the one outlined here.

The probability that any asteroid is a NEA may be determined based solely on its rates of motion. This method allows a discovery program to determine beforehand a false detection rate of NEAs and, by considering the time required for followup of each candidate, maximize the discovery rate in terms of the confidence level cutoff on the NEA identification. Implementation of this technique reduces the bias inherent to the data, simplifying analysis of the discoveries. The Spacewatch results are in good agreement with the present calculations.

A system similar to the 0.9 m Spacewatch telescope with a limiting magnitude of 21, searching for NEAs larger than about 500 m diameter, will be most effective at finding them towards opposition. Larger aperture systems (such as the new 1.8 m Spacewatch Telescope currently under construction) may find that it is most effective to search about 45° east or west of opposition due to the increased volume of NEA space which is searched, and the increase of brightness for asteroids at constant geocentric distance but increasing phase angle.

This work has been supported by grants from AFOSR and NASA to Professor Tom Gehrels. The author would also like to thank Bill Bottke, Dan Durda, Tom Gehrels, Bob McMillan, Travis Metcalfe, David Rabinowitz, Jim Scotti, and Mark Sykes for assistance in this research.

## REFERENCES

Bowell, E., Hapke, B., Domingue, D., Lumme, K., Peltoniemi, J., & Harris, A. W. 1989, Asteroids II, edited by R. Binzel, T. Gehrels, and M. S. Matthews (The University of Arizona Press, Tucson), p. 524

Bowell, E., Skiff, B., & Wasserman, L. 1990, Asteroids, Comets, Meteors III, edited by C. I. Lagerkvist, H. Rickman, B. A. Lindblad, and M. Lindgren (Uppsala Universitet, Uppsala), p. 19

Bowell, E., & Muinonen, K., 1994, Hazards Due to Comets and Asteroids, edited by T. Gehrels (The University of Arizona Press, Tucson, AZ), p. 149

Durda, D., & Dermott, S.F. 1995, Icarus, in preparation

Gehrels, T., & Jedicke, R. 1995, in Earth, Moon and Planets (Kluwer Academic, The Netherlands), Vol. 71, pp. 233–242

Hills, J. G., & Leonard, P. J. T. 1995, AJ, 109, 401

Moulton, F. R. 1914, An Introduction to Celestial Mechanics (MacMillan, New York), p. 185

Rabinowitz, D. L. 1991, AJ, 101, 1518

Rabinowitz, D. L., *et al.* 1993, Nature, 363, 704

Rabinowitz, D. L. 1994, Icarus, 111, 364

Rabinowitz, D. L., Bowell, E., Shoemaker, E., & Muinonen, K. 1994, Hazards Due to Comets and Asteroids, edited by T. Gehrels (The University of Arizona Press, Tucson, AZ), p. 285

Shoemaker, E. M., Shoemaker, C. S., & Wolfe, R. F. 1989, Asteroids II, edited by R. Binzel, T. Gehrels, and M. S. Matthews (The University of Arizona Press, Tucson), p. 487

Tholen, D. J., & Barucci, M. A. 1989, Asteroids II, edited by R. Binzel, T. Gehrels, and M. S. Matthews (The University of Arizona Press, Tucson), p. 298

Van Houten, C. J., Van Houten-Groeneveld, I., Herget, P., & Gehrels, T. 1970, A&AS, 2, 339

Zellner, B., Thirunagari, A., & Bender, D. 1985, Icarus, 62, 505